Geomorphology 131 (2011) 69–84

Contents lists available at ScienceDirect

Geomorphology

journal homepage: www.elsevier.com/locate/geomorph

Megaripple flattening due to strong winds

Ori Isenberg [a], Hezi Yizhaq [a,*], Haim Tsoar [b], Rimon Wenkart [b], Arnon Karnieli [a], Jasper F. Kok [c], Itzhak Katra [b]

[a] Institute for Dryland Environmental Research, Jacob Blaustein Institutes for Desert Research, Ben-Gurion University of the Negev, Sede Boqer Campus, 84990, Israel
[b] The Department of Geography and Environmental Development, Ben-Gurion University of the Negev, Beer Sheva, 84105, Israel
[c] Advanced Study Program, National Center for Atmospheric Research, Boulder, CO, 80307, USA

ARTICLE INFO

Article history:
Received 29 August 2010
Received in revised form 21 April 2011
Accepted 24 April 2011
Available online 30 April 2011

Keywords:
Megaripples
Sand ripples
DEM
Photogrammetry
Drift potential (DP)
COMSALT

ABSTRACT

Megaripples in Nahal Kasuy in the southern Negev Desert of Israel are characterized by a mean wavelength of about 70 cm and by a bimodal distribution of coarse and fine particle sizes, the latter property being a prerequisite for their formation. In our three-year project, megaripple development was monitored using a digital elevation model (DEM) constructed from above-ground stereo digital photographs. Temporal dynamics of wind power (drift potential, DP) were measured, and grain-size analyses were performed on samples taken from different parts of the megaripple. The coarse grains that protect the crest enable the ripple to grow, but when ripple height becomes too high, the bed shear stress increases, thus allowing the wind to move the armoring layer. When this happens (during strong wind storms) the megaripple will flatten and even disappear, as was observed in our field study. We present measurements that for the first time directly show the megaripple to normal ripple transition, and we suggest two possible physical processes as potential causes of this phenomenon. Megaripple flattening can occur either when the wind exceeds the fluid threshold for a sufficient length of time or after a sequence of storms with winds blowing from the same direction.

1. Introduction

Aeolian ripples larger and higher than those commonly found in fine sand are known by various names, including ridges (Bagnold, 1941), granule ripples (Sharp, 1963), gravel ripples (Sakamoto-Arnold, 1988), or megaripples (Ellwood et al., 1975; Greeley and Iversen, 1985). Large aeolian sand ripples on Earth have been described in many places, among them the Kelso Dunes and Coachella Valley sands in Southern California (Sharp, 1963), in the Libyan desert (Bagnold, 1941; El-Baz, 1986), the northern Sinai (Tsoar, 1990), Swakopmund, Namibia, (Fryberger et al., 1992), northeastern Iceland (Mountney and Russell, 2004), and on the coast of northeastern Brazil (Yizhaq, 2008). More examples are presented in Fig. 1. Enormous megaripples were recently documented in Carachi Pampa, Argentina, at a height of 4000 m above mean sea level (Milana, 2009). Composed of volcanic pebbles, these megaripples were formed by the action of extremely strong winds (probably the strongest winds known on Earth, ~400 km/h). Megaripple wavelengths were up to 43 m and their heights were about 2.3 m (Milana, 2009) with a crest maximum grain size of 19 mm. Megaripples and aeolian bedforms that are known as Transverse Aeolian Ridges (TARs) are also abundant on Mars (Balme et al., 2008; Zimbelman et al., 2009), and it is still unknown whether these unique bedforms are large megaripples or transverse dunes. Various applications of sand ripple studies on Earth and Mars were reviewed by Rubin (2006).

There are correlations between megaripple wavelength λ and height h (given by the ripple index RI defined as $RI = \lambda/h$, of approximately 15) and between wavelength and maximum particle size (Pelletier, 2009; see also Figs. 3 and 4 in Williams et al., 2002). The larger the maximum particle size, the larger the wavelength, although the dependence is probably nonlinear. Therefore, Stone and Summers (1972) suggested that the relationship can be described by $\lambda = 63.8D^{0.75}$. Here, D (mm) is the average diameter of sand on the crest of ripples and λ (cm) is the wavelength. However, this formula has been never confirmed by other studies.

According to Bagnold (1941), it may take decades or centuries to form huge megaripples, with their dimensions varying as the square root of age. However, from his studies of the Kelso Dunes, Sharp (1963) suggested that with a large enough supply of coarse grains, it may take only weeks for well-defined granule ripples to form. It was also observed that during a severe windstorm in the southern San Joaquin Valley in California, megaripples formed on a timescale of hours or days (Sakamoto-Arnold, 1988). For large megaripple bedforms to develop, a bimodal distribution of particle sizes seems to be required, as was shown by Sharp (1963), who found that coarse grains comprise 50–80% of the crest material and less than 10–20% of the trough. For more detailed information about wind tunnel and field

* Corresponding author. Tel.: +972 8 6596789; fax: +972 8 6596921.
E-mail address: yiyeh@bgu.ac.il (H. Yizhaq).

0169-555X/$ – see front matter © 2011 Elsevier B.V. All rights reserved.
doi:10.1016/j.geomorph.2011.04.028

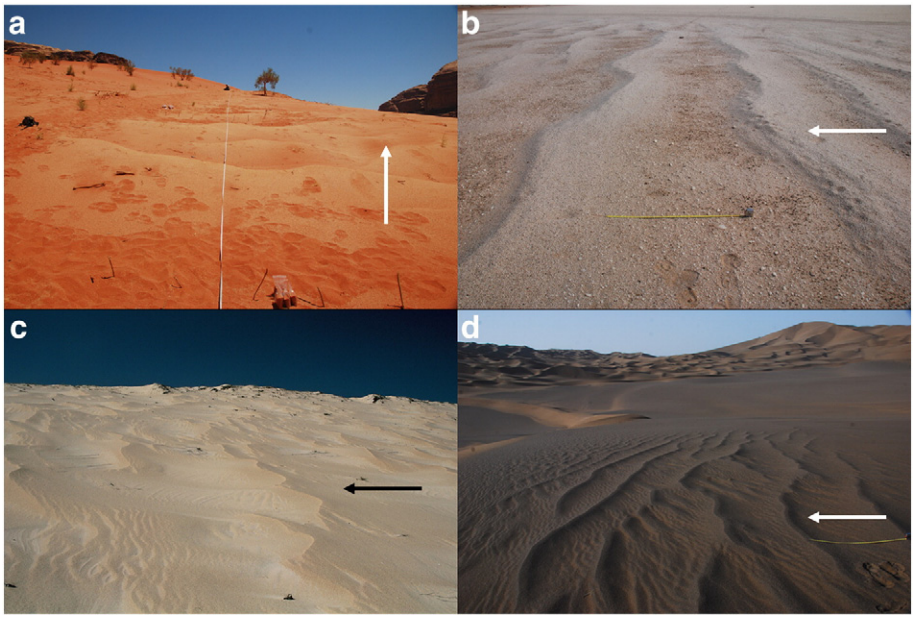

Fig. 1. (a) Aeolian megaripples in Wadi Rum, Jordan. The megaripple mean wavelength was about 2.17 m and the mean height was 20 cm. Normal sand ripples can be seen in the troughs. The arrow indicates the direction of the prevailing wind. (b) Megaripples along the Skeleton Coast, Namibia. The average wavelength was about 2 m and the average height was about 10 cm. (c) Aeolian sand megaripples along the Ceará coast in Northeastern Brazil. The wavelength was more than 3 m (the length of the measuring strip) and the height was about 50 cm. The diameter of the coarse grains that cover the ripple crest was about 3 mm. The average wind velocity during the dry season was 7.75 m/s (Jimenez et al., 1999). Note that normal ripples (arrow) have developed in the troughs between the megaripples. (d) Megaripples in the Sanshan Desert, western Xinjiang, China. The average wavelength was about 1 m (see the scale in the figure).

experiments, we refer the reader to Yizhaq (2008) and to Yizhaq et al. (2009).

Recent studies of megaripples (Milana, 2009; Yizhaq et al., 2009; Zimbelman et al., 2009) have left many questions unanswered regarding their formation. Basically, it is still not known whether megaripples continue to grow indefinitely or whether they reach saturation, and how the interplay between wind and grain size distribution dictates the wavelength. In addition, it is not clear whether the impact mechanism is also responsible for the huge megaripples observed at Puna Plateau in Argentina (MIlana, 2009) or on Mars (Zimbelman et al., 2009). In the current work we study how strong storms can destroy megaripples, and thus, we offer a partial answer to the question about wavelength saturation.

2. Material and methods

2.1. Research area

Our field experiment was carried out on the Nahal (wadi) Kasuy sand dunes in the southern Negev (Fig. 2) that cover an area of 15 km^2 (Ginat, 1991). Southwestern storm winds cause the sand to drift into Nahal Kasuy from the Uvda Valley and pile up in the wadi bed (Fig. 2). Annual precipitation in Nahal Kasuy is about 37 mm, and shrubs of *Haloxylon persicum* that sparsely cover the wadi bed constitute the most prominent vegetation.

The megaripple field is located in the middle of the wadi, where coarse grains abound. Mean megaripple wavelength is about 70 cm, with a mean height of about 7 cm ($RI \sim 10$). Smaller ripples reflecting the direction of the most recent wind are superimposed on the megaripples. Compared to those in other parts of the world, the Kasuy megaripples are small (Fig. 1), and therefore, they are expected to be more sensitive to the storms that form and modify them and that can even destroy them.

To study megaripple evolution, we flattened three plots and hand mixed the grains to achieve uniform distributions of coarse and fine grains. Plot sizes and flattening dates are given in Table 1 (see Fig. 2c). The fourth (D) and the fifth (E) plots were not flattened but were marked to track the changes of the large and medium size megaripples, and therefore, they can be considered control plots. In this paper we only show results from plot D; for results from the other plots, see Yizhaq et al. (2009).

2.2. Wind-speed measurements

Measurements of wind speed and direction at a height of 3.3 m were made using two anemometer recorders that were placed at the eastern edge of the megaripple field. The wind speed was used to calculate drift potential (DP) and resultant drift potential (RDP) (Fryberger, 1979). Theoretical and empirical studies have shown that the potential volume of sand transported by the wind per unit time through a 1 m-wide cross-section is proportional to DP (Fryberger, 1979; Bullard 1997). DP is calculated from:

$$\mathrm{DP} = \langle u^2(u - u_t)\rangle, \tag{1}$$

where u is the wind speed (in knots; 1 knot = 0.514 m/s) measured at a height of 10 m and the angle brackets denote an average on time; and u_t is the minimal threshold velocity (12 knots = 6.17 m/s) necessary for the transport of a typical sand grain (with an average diameter of 0.25 mm) (Fryberger, 1979).

RDP is the vector summation of DP from different directions and over the n measurements. Mathematically, it can be written as:

$$\mathrm{RDP} = \sqrt{\mathrm{RDP}_x^2 + \mathrm{RDP}_y^2}$$

where $\mathrm{RDP}_x = \sum_{i=1}^{n} \mathrm{DP}_i \cos\theta_i$, $\mathrm{RDP}_y = \sum_{i=1}^{n} \mathrm{DP}_i \sin\theta_i$, and θ_i is related to the wind direction. The direction of RDP is referred to as the resultant drift direction RDD, which is defined as $\mathrm{RDD} = \arctan(\mathrm{RDD}_y / \mathrm{RDD}_x)$. RDD expresses the net trend of sand drift, namely, the direction

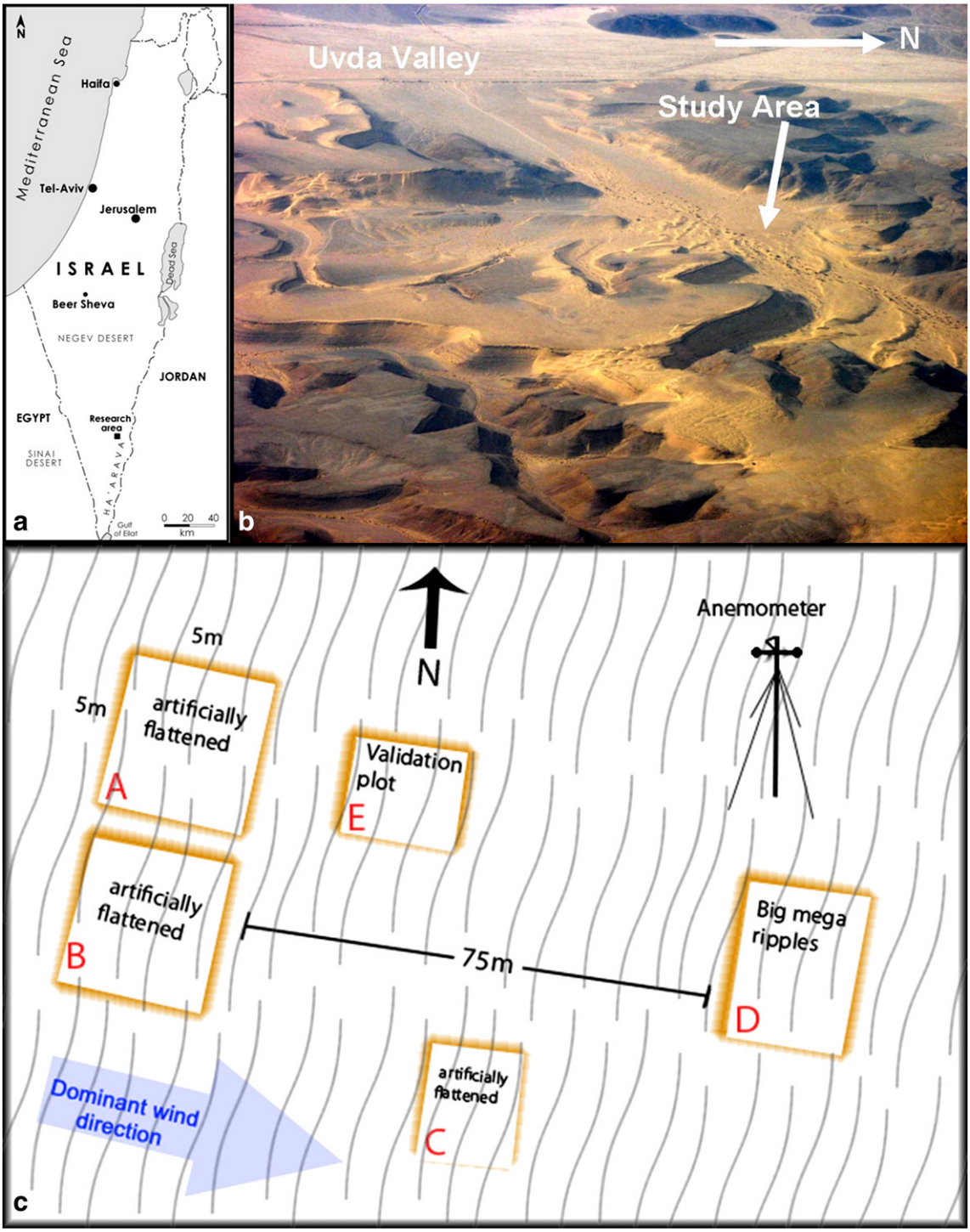

Fig. 2. (a) The research area (indicated by a black square) is located in the southern Negev, 46 km north of the Gulf of Eilat. (b) An aerial photo of Nahal Kasuy. The megaripples were located in the middle of the wadi (indicated by the white arrow; their location was 29° 59′ 14″ N; 34° 59′ 25″ E, 430 m above mean sea level). (c) Schematic map of the plots at Nahal Kasuy. Plots A, B, and C were artificially flattened and Plots D and E were used to track megaripple spatial dynamics.

Table 1
Plot descriptions.

Plot	Begin treatment date and characteristics	Size
A	Flattened in January 2008 and marked with iron rods that indicated Ground Control Points.	5×5 m
B	Flattened in January 2007	5.5×5.5 m
C	Flattened in November 2006	4×4 m
D	March 2008, large megaripples	5×5 m
E	June 2008, medium megaripples	5×3 m

in which sand would drift under the influence of winds blowing from various directions. The ratio of RDP to DP (RDP/DP) is an index of the directional variability of the wind (e.g., RDP/DP = 1 stands for unidirectional wind, and RDP/DP = 0 characterizes multidirectional winds that vectorially cancel each other out). DP is the potential sand drift, but the actual sand drift potential depends further still on the mean grain diameter, the degree of surface roughness, the amount of vegetation cover, and sand moisture.

To determine DP, the wind speed at a height of 10 m must be calculated, which can be done using the Karman–Prandtl velocity distribution equation (Greeley and Iversen, 1985),

$$\frac{u}{u_*} = \frac{1}{\kappa} ln\frac{z}{z_0}, \quad (2)$$

where κ is von Karman's constant (=0.4), u is the wind speed at height z, u^* is the shear velocity, and z_0 is the aerodynamic roughness. According to Bagnold (1941), $z_0 \approx d/30$, where d is the mean grain diameter, assuming well-sorted particles with homogenous, flat surfaces. The value of z_0 also depends on the particle size and spacing (Greeley and Iversen, 1985), and it can be as large as $d/8$. Using wind speed measurements taken at a height of 3.3 m ($u_{3.3}$) together with Eq. 2 and the estimated value of z_0, the wind speed at the standard height of 10 m (u_{10}) can be calculated from:

$$u_{10} = \frac{u_{3.3}\ ln(10/z_0)}{ln(3.3/z_0)}. \quad (3)$$

To obtain DP, we used $z_0 = d/25$ with $d = 0.25$ mm [the standard diameter (Fryberger, 1979)], which is the mean grain diameter typically used for such calculations. For these values, the correction factor $\ln(10/z_0)/\ln(3.3/z_0)$ is 1.1. We also compared our results with wind measurements conducted at the meteorological station located at Uvda airport (30N, 34.883E; 3 km west of Nahal Kasuy), and there is good agreement between the two sets of measurements. Note that Eq. 3 is valid only in the absence of saltation. When saltation is occurring, z_0 should be replaced by the larger saltation roughness length.

2.3. Photogrammetry

To produce digital photographs, we used red–green–blue (RGB) images from a digital Nikon D80 camera with a Sigma 10–20 mm lens. Processing took place with Erdas Imagine ver. 9.1 and its Leica Photogrammetry Software (LPS) extension. Use of a small focal-length lens of 10 mm, which corresponds to a 94.5° field of view, effectively reduced the number of photographs needed to cover the plots. To avoid interfering with plot dynamics, the imaging and the ground control point (GCP) markings had to be made from outside the plot. The camera, which was mounted on a special 5 m-long rail fixed to a tripod on either end, could be moved along the rail by two cords attached to it. We used a remote control cable to operate the camera.

Initially, the GCPs were used for geometrical rectification. In principle, GCPs could be placed outside the plots to derive a digital elevation model (DEM) with photogrammetry. This method was used in Plot A, and involved vertically inserting iron rods 0.6 mm in diameter and 12 cm long into the ground at specific, well-defined points. The rods give the x, y and z (height) coordinates. We decided to use long rods instead of flat GCP panels because of the constantly changing surface levels, which cause the GCP panels to become covered by sand.

To acquire an accurate DEM, however, we found that for our work, the GCPs had to be placed throughout the plots. Briefly, the method that was used in the other plots (B, C, D and E) involved marking the surface with holes using a giant "comb". The 5 m-long comb pinched the surface and left marks on the sand at 15 cm intervals that were used as GCPs. The locations of the holes made by the comb give only the x and y coordinates, but not the z values. We ensured that the comb marks were always in the same locations as the iron rods by placing the comb in the same starting points as marked by the iron pegs. All plots were photographed once every three weeks.

2.3.1. Processing and analysis

Image analyses were carried out with the LPS Project Manager. To reduce the need for a large number of GCPs for each plot, the LPS Project Manager uses the self-calibrating bundle block adjustment method. With this approach, the internal geometry of each image and the relationship between overlapping images is determined with a small number of GCPs.

The only manual process needed to implement this approach is geometric rectification, after which the program automatically extracts all the data needed for the "Automatic Terrain Extraction" feature embedded in the LPS. The main photogrammetry output we used in this study was the DEM that provided the two most important parameters in ripple measurement, i.e. wavelength and ripple height. Measuring these parameters together with continuous wind measurements enabled us to track temporal topographic changes.

DEM quality depended on many factors. We obtained the best results when images where taken in the late afternoon when contrast was maximized. By selecting the camera's Auto Mode option, aperture and shutter speed were chosen automatically; no significant deviations in color or hue were noticed among the pictures.

Fig. 3 shows typical megaripples at Nahal Kasuy and the DEM profiles of four ripples.

To analyze the average distance movement $\overline{d}$ that megaripples moved, we used the following method (Levin and Ben-Dor, 2004):

$$\overline{d} = \frac{1}{n}\sum_{i=1}^{n} d_i \quad (4)$$

where d_i is the distance along the normal to two successive crest lines and n is their number (see Fig. 4).

The average distance of megaripple drift due to wind and the wind speed measurements allow us to calculate the creep mass flux particles q_c (in kg m/s) using the following formula (Jerolmack et al., 2006; Zimbelman et al., 2009):

$$q_c = (1-p)\rho cH/2 \quad (5)$$

where p is the porosity, ρ is the particle density (in kg/m^3), c is the ripple migration (in m/s) rate, and H(in m) is the ripple height. While using Eq. 5, we assumed that the ripple height remained unchanged.

2.3.2. Validation

To validate measurement scale correctness, we used a mechanical profiler, based on the principle of a "nail board" that can capture the structures of the ripples measured with the DEM method. This procedure helped us accurately compare the digital and true ripple profiles. Fig. 5 (a and b) shows two profile curves of megaripples in plot E, one done with the profiler and the second with the photogrammetry technique. For validation, we also used a piece of asbestos with a uniform wavy surface (Fig. 5c). In both cases the DEM method gave good results [for more details, see Yizhaq (2008)].

2.4. Grain-size analysis and its importance

Samples of sand were retrieved from the field study with a tin can (diameter 84 mm, height 35 mm) by pressing the can into the cross-section of the megaripple under study. Samples were obtained from the trough, the windward face, the crest, and the leeward slope and from incipient megaripples ($\lambda = 0.15$ m). The samples were scooped out of the can with a flat scraper. All samples from Nahal Kasuy were taken on the same day (5th February 2008). We also took ten samples from nearby normal sand ripples to compare with those of the megaripples and 32 samples from two larger megaripples from Wadi Rum in Jordan on 25th July 2008 (see Fig. 1a) from the bottom and the middle of a windward dune slope. It is important to note that all the samples were taken using the same method. Average sample weight was 310 g (with values ranging between 282 and 336 g). Each sample was divided in half by a splitter. Grain-size distribution was obtained using standard sieves suspended on a shaker. The aperture of each

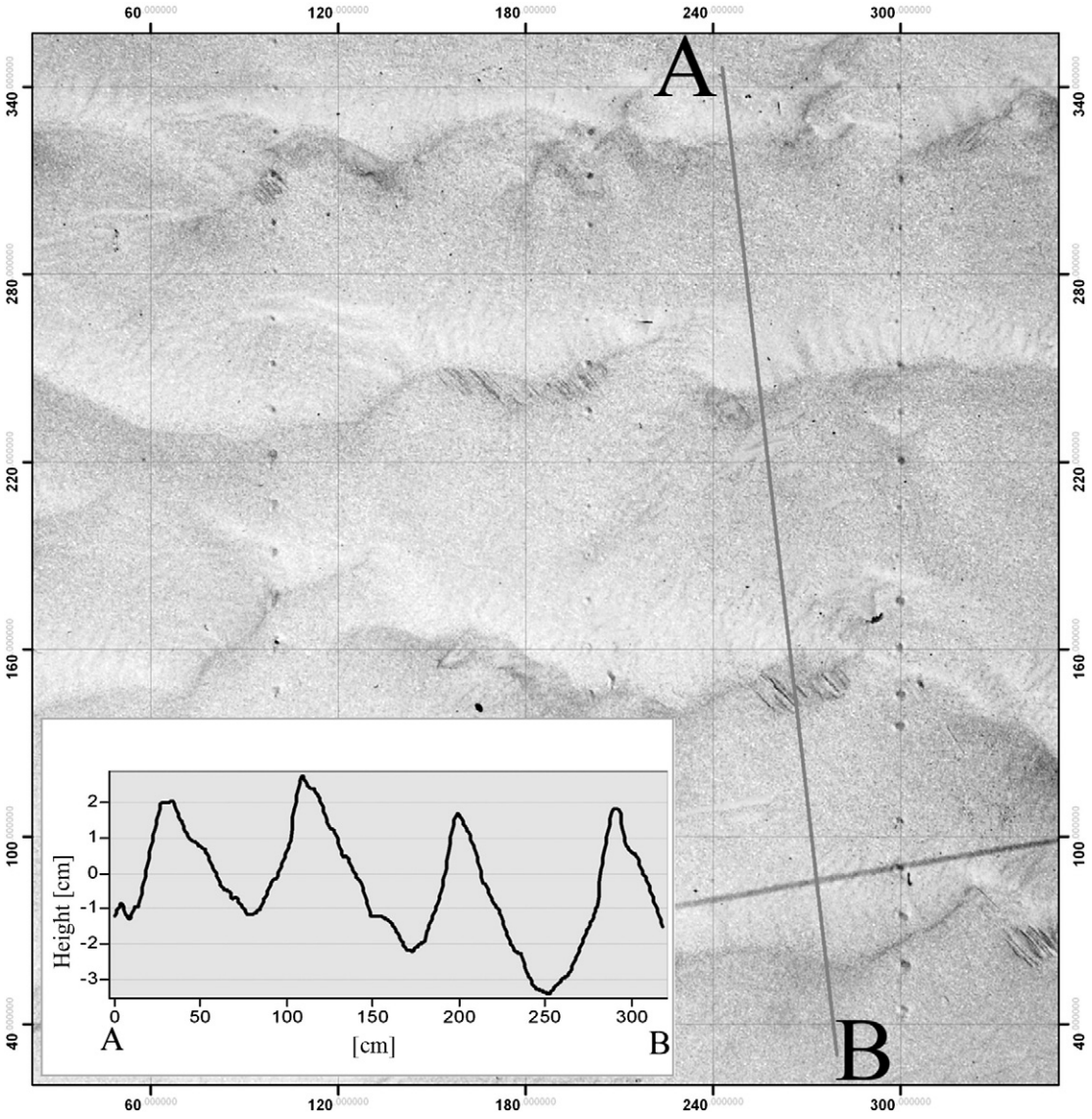

Fig. 3. Typical megaripples at Nahal Kasuy (the square grid is 60 × 60 cm). The inset shows the photogrammetry profile along a cross-section (line AB). The average wavelength was 70 cm and the average height was about 4 cm (the wind direction was from B to A).

sieve was greater by 1/4 ϕ than the one above it ($\phi = -\log_2 d$ where d is the grain diameter).

In addition, samples were taken from six saltation traps located near the plots on 23rd March 2008 and again one week later. These latter samples are associated with two strong wind storms that occurred during March 2009. For these samples, particle size distribution (PSD) analysis was performed by ANALYSETTE 22 MicroTec Plus laser diffraction. The instrument measures particle size over the range of 0.08 to 2000 μm. The preparation of each soil sample included sample splitting for replicate samples by a micro-splitter device, sieving to <2000 μm (the upper portion was weighed and recorded), and the removal of distinct organic matter. For the PSD

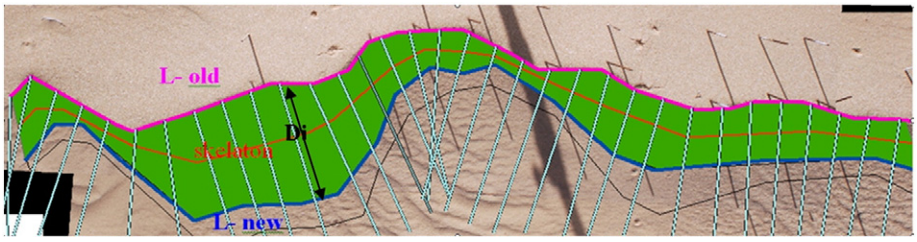

Fig. 4. Schematic illustration of the method used to analyze average ripple movement between two successive measurement times. For this example, the normal to the crests defined as d_i in Eq. 5 was 20.58 cm.

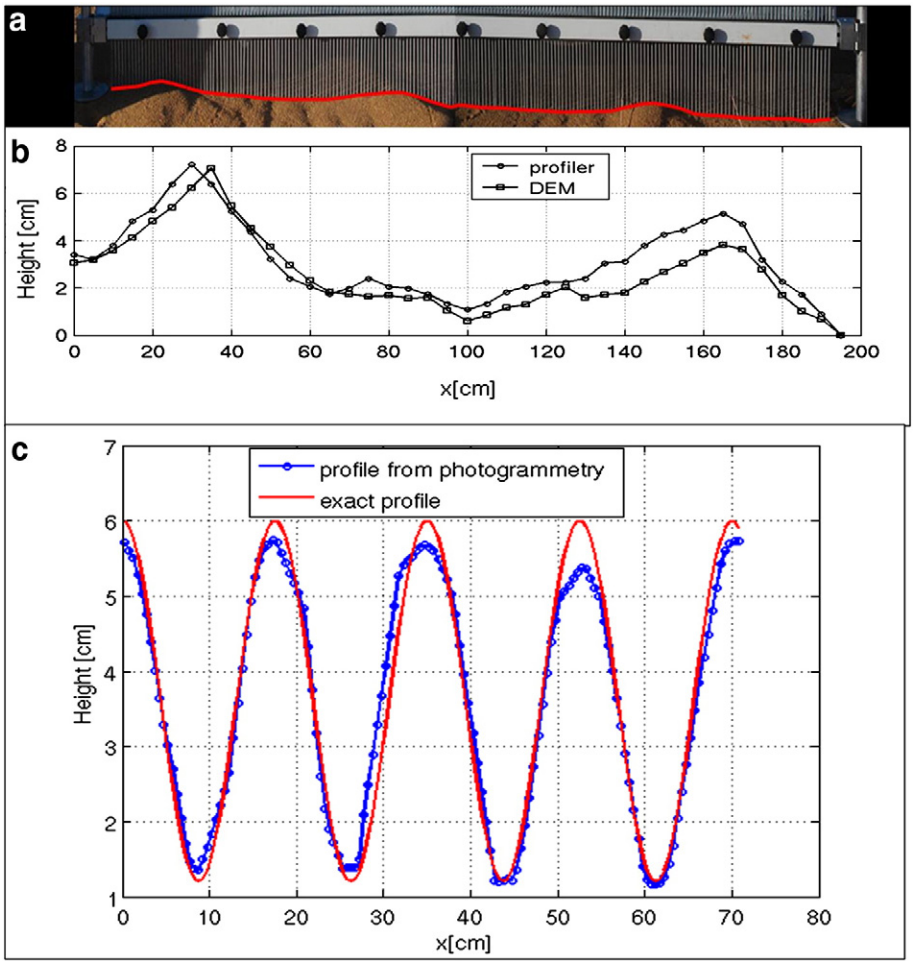

Fig. 5. (a) The profiler used to measure megaripple profiles in plot E. (b) The measured and DEM profiles are shown together. (The wind direction is from left to right.) The agreement between the two is highly satisfactory (the average error was about 2%). (c) Validation using a piece of asbestos with a wavy surface. Also in this case there was good agreement between the DEM method and direct measurement (the average error was about 1%).

analysis, three replicate samples (4 to 5 g) of each soil sample were dispersed in a Na-hexametaphosphate solution (at 0.5%). The PSD data were calculated using the Fraunhofer diffraction model due to the negligible number of clay-sized particles in the sandy soil.

The grain-size analysis also contributes to the understanding of megaripple formation by enabling an estimation of the threshold velocity needed to dislodge the coarse grains on the dune crest. According to Bagnold (1941), the threshold shear velocity is given by:

$$u_{*t} = A\sqrt{\frac{\rho_s - \rho}{\rho} g d} \tag{6}$$

where ρ_s is the grain density (taken as 2710 kg/m^3), ρ is the air density (taken as 1.2 kg/m^3), g is the acceleration of gravity, and d is the grain diameter, with A being a coefficient ($A \approx 0.1$) that depends on the grain Reynolds number (Pye and Tsoar, 2009). Eq. 6 is not valid for grains smaller than 0.1 mm due to the inter-particle cohesive forces that become important for the smaller grains. Also, A is not constant for finer sands (Pye and Tsoar, 2009).

Using Eqs. (2) and (6) gives the threshold velocity u_t at height z,

$$u_t = \frac{1}{\kappa} A \left(\frac{(\rho_s - \rho) g d}{\rho}\right)^{1/2} ln(z/z_0) \tag{7}$$

According to Shao and Lu (2000) the critical threshold for the initiation of motion for static grains (shear velocity) is given by:

$$u_{*t} = \sqrt{0.0123\left(sgd + \frac{3 \times 10^{-4}}{\rho d}\right)} \tag{8}$$

where s is the ratio between the sediment density and the fluid density. Fig. 7 compares the two equations of Bagnold with the Shao and Lu equation (2000) for threshold wind velocity at the height of 3.3 m using $z_0 = d/25$. Note that the threshold velocity according to Eq. 8 is always higher than that calculated by the Bagnold equation.

Eqs. 6 and 8 are estimations of the threshold shear velocity as they are only correct for a unimodal distribution of identical grains. This is not the case for the megaripple crest. For mixed size grains, the critical shear velocity may be much smaller for coarse grains on a bed composed primarily of fine particles (Fenton and Abbott, 1977; Raudkivi and Ettema, 1982; Jerolmack et al., 2006), as the coarse grains are more exposed to the wind and because the angle of repose is smaller for a coarse grain resting upon fine grains (Wiberg and Smith, 1987). In addition, we assume that the grain entrainment occurs due to the drag and lift forces of the moving air (a mechanism that works through a fluid threshold). The fluid threshold velocity is the upper limit for grain entrainment because the impact of the saltating grains can drive other grains into saltation when the wind is above an impact-driven threshold which is about 0.82 of the fluid threshold (Anderson and Haff, 1988;

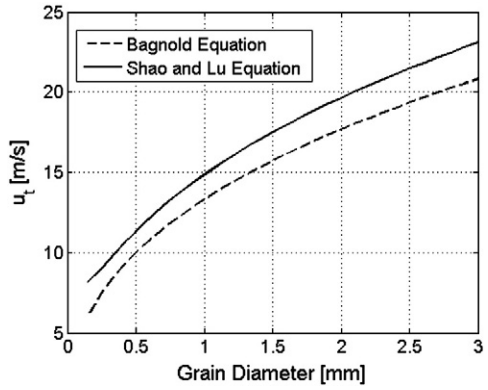

Fig. 6. Threshold velocities at height 3.3 m according to Eqs. 6 and 8 as a function of the grain diameter for different z_0 values. Parameter values: $A=0.1$, $\kappa=0.4$, $\rho_s=2710$ kg/m^3 (calcite), $\rho=1.2$ kg/m^3, and $g=9.8$ m/s^2 (Defoe and Compton, 1925).

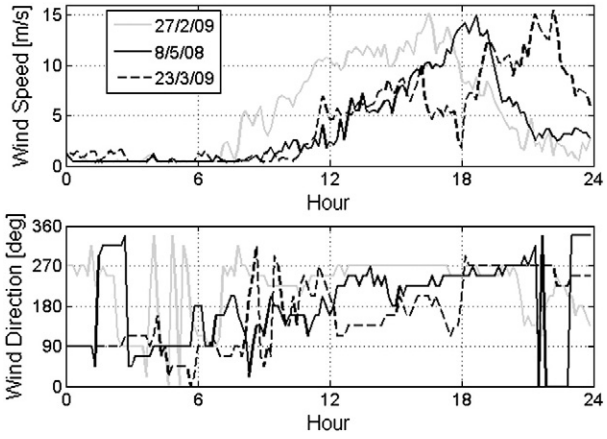

Fig. 8. Recordings of the three strongest storms at Nahal Kasuy during the research (8th May 2008 and 27th February and 23rd March 2009) at 10-min intervals, measured at 3.3 m. The three storms exhibited maximum speeds of approximately 15 m/s, the highest wind speed measured during the study.

Kok, 2010a, 2010b). Nevertheless, Fig. 6 provides important information about the wind speed necessary for coarse-grain saltation, which can remove the megaripple armoring layer and break it into small ripples, as suggested by Ellwood et al. (1975).

3. Results and discussion

3.1. Winds at Nahal Kasuy

Fig. 7 summarizes wind speed measurements for the years 2007–2009. The corresponding values for DP in Nahal Kasuy during the research were very low (48.7 v.u. in 2007, 39.6 v.u. in 2008, and 53.2 v.u. in 2009). Compared to DP measurements for the nearby Uvda airport (30′N. 34.883′E), data from 2008 included the lowest recorded value for DP since 1986.

The windiest months are January to May, with the prevailing winds coming from the southwest. During the summer and fall the wind is much less intense and there is almost no sand transport in the study area. According to Fryberger's (1979) classification, Nahal Kasuy is a low-wind environment (DP<200), a contributing factor to understanding the following results.

Due to the cubic dependence of DP on the wind speed, storm events dramatically increase sand transport and significantly impact the ripple field. Fig. 8 shows the three most significant windstorms that occurred during our research. For all three storm events, measurements made at a height of 3.3 m revealed that the winds were westerly and had a maximum velocity of 15 m/s. Moreover, consistent with the general pattern in Israel, the highest wind speeds during the storms occurred in the afternoon and evening (Goldreich, 1998) and showed typical diurnal variation (Manwell et al., 2009).

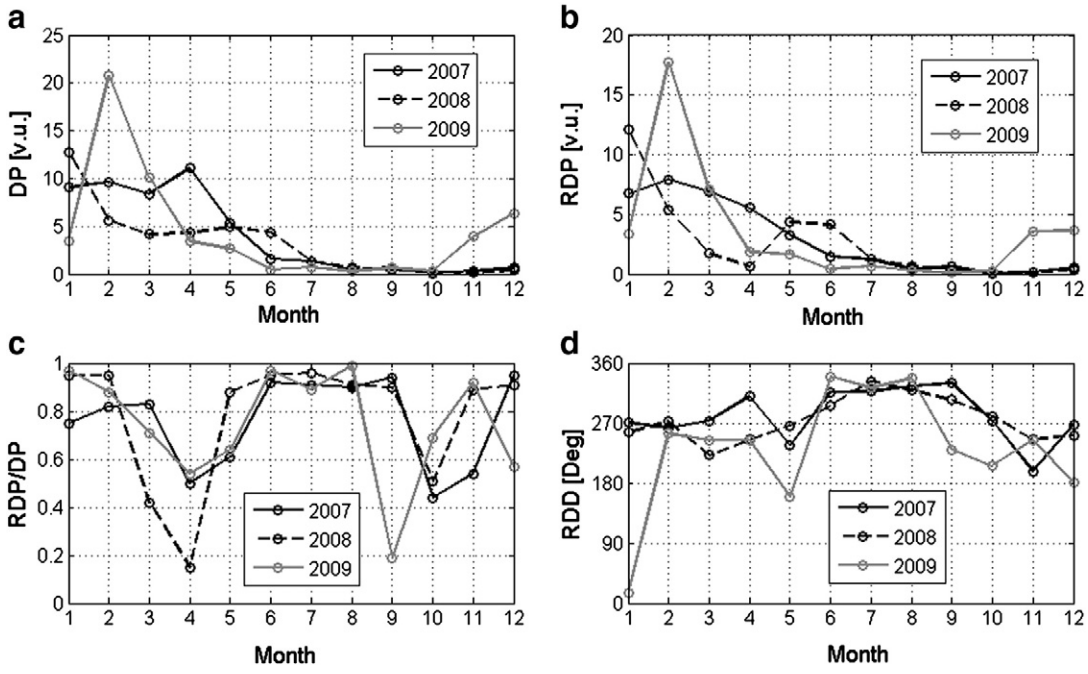

Fig. 7. Summary of wind speed measurements at Nahal Kasuy for the years 2007–2009 based on 10-min intervals. (a) Drift Potential (DP) per month in annual values. (b) Resultant drift potential (RDP). (c) Ratio RDP/DP that expresses the variability in the wind direction. (d) Direction of the resultant drift potential (RDD).

Daily variations in solar radiation are responsible for diurnal wind variations in temperate latitudes over relatively flat land areas.

We used wind speed data from the years 2008–2009 (time resolution of 10 min) to extract an approximation to the Weibull distribution (Manwell et al., 2009) defined as:

$$p(U) = \left(\frac{k}{c}\right)\left(\frac{U}{c}\right)^{k-1} \exp\left[-\left(\frac{U}{c}\right)^{k}\right] \tag{9}$$

where U is the wind speed (we used the wind measurements at 3.3 m), k is the shape factor, and c is the scale factor. Both of the latter two parameters are functions of average wind speed ($\bar{U}$) and standard deviation (σ_U) that can be approximated by (Manwell et al., 2009):

$$k = \left(\frac{\sigma_U}{\overline{U}}\right)^{-1.086}$$
$$c = \overline{U}(0.568 + 0.433/k)^{-1/k} \tag{10}$$

Based on our data set, $\bar{U} = 2.56$ m/s, $\sigma_U = 1.86$ m/s, $k = 1.42$, and $c = 2.82$. Fig. 9 shows the wind distribution density function and its Weibull distribution. Solving the cumulative distribution function (Manwell et al., 2009), which represents the probability that the wind speed is less than or equal to a given wind speed, given by:

$$F(U) = 1 - \exp\left[-\left(\frac{U}{c}\right)^{k}\right] \tag{11}$$

showed that with a probability of 99.9%, the wind speed in Nahal Kasuy was less than or equal to 11 m/s, which is less than the threshold velocity for coarse particles located on the ripple crest. This result has important implications for megaripple morphodynamics, as we show in Section 3.3.

3.2. Grain-size analysis

In a previous work (Yizhaq et al., 2009) we presented the results of grain-size analysis in detail. In the current study, we compared the megaripples of Nahal Kasuy and Wadi Rum (southern Jordan), taking samples only from the crests. Fig. 10 and Table 2 present the main characteristics of megaripples, sampled along the profile, in Nahal Kasuy and in Wadi Rum.

The sorting (standard deviation) column in Table 2 refers to the range of grain size. Better sorted sediments have lower σ_ϕ values. Samples were taken from depths of up to 35 mm, and the grain size range was largest at the megaripple crest, the upper layer of which exhibited the coarsest grains while finer particles lay underneath, both in Nahal Kasuy and in Wadi Rum. Normal ripple samples, in contrast, were well sorted and showed a unimodal distribution. These results support Walker's (1981) conclusion that ripple wavelength also depends on sorting and can increase as sorting deteriorates, i.e., the difference between the coarsest and finer particles increases.

Skewness (Sk_ϕ) is one of the more sensitive parameters for sediment characterization. Positive Sk_ϕ values indicate that the distribution has a more pronounced tail of fine material compared with a log-normal distribution. Conversely, negative Sk_ϕ values indicate a tail of coarser particles or a deficiency of fine particles compared with log-normal distribution (Pye and Tsoar, 2009).

According to Table 1 and the classification by Blott and Pye (2001), the samples taken from the normal ripples are very finely skewed, the samples taken from the megaripples are finely skewed, and those from the incipient megaripples and from Wadi Rum are symmetrical.

Kurtosis measures the 'peakedness' of the distribution. Frequency distributions that are flatter than a normal probability curve are referred to as platykurtic and strongly peaked curves are described as leptokurtic (Pye and Tsoar, 2009). Normal ripple samples show the most pronounced 'peakedness', whereas the samples from the megaripples are platykurtic and even mesokurtic, i.e., their frequency curves are flatter than the normal distribution.

Fig. 10 shows the grain size distributions across the ripple profile for megaripples at Nahal Kasuy and Wadi Rum. The grain diameter relating to the local maximum in the distribution curve is the mode. In Nahal Kasuy, the coarser mode at the crest was $d = 780$ μm, whereas the finer mode of the trough sample was $d = 115.5$ μm. The overall distribution between the small megaripples at Nahal Kasuy and large megaripples at Wadi Rum was the same, but there was a significant shift to the coarser grains at the latter (the shift was observed for both coarse and the fine modes). The coarse mode for the crest sample at Wadi Rum was $d = 1850$ μm while the fine mode was $d = 375.5$ μm. This shift to coarser grains was also evident in other parts of the cross-section, on both windward and leeward slopes. These results indicate that the larger the coarse particles that cover the crest, the larger the megaripple wavelength—a finding that is in agreement with former studies (Stone and Summers, 1972; Williams et al., 2002).

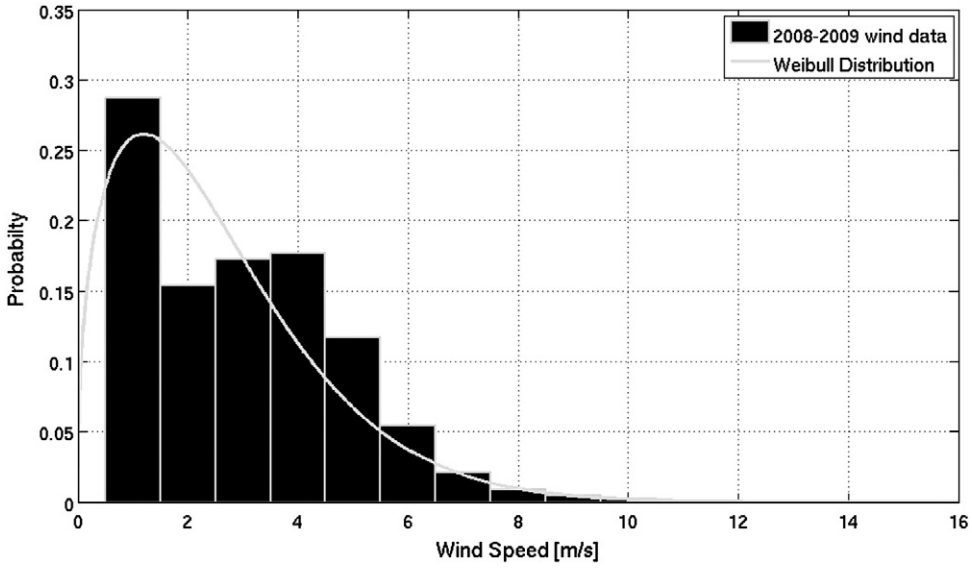

Fig. 9. Wind probability density function for the years 2008–2009 and the Weibull approximation according to Eqs. 8 and 9. The average wind speed for this period was a relatively low 2.56 m/s and was measured at a height of 3.3 m.

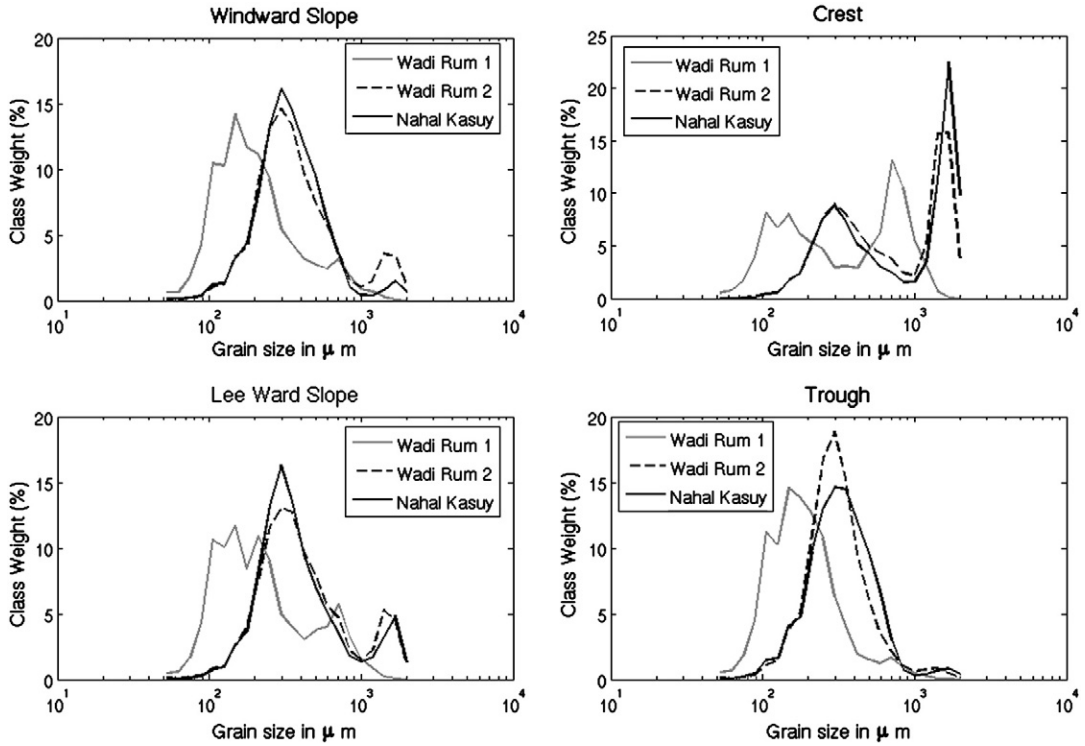

Fig. 10. Average grain size distributions of samples taken from megaripple windward faces, crests, leeward slopes, and troughs in Nahal Kasuy and in Wadi Rum. In Nahal Kasuy, the coarser mode at the crest was $d = 780$ μm whereas the finer mode from the trough sample was $d = 115.5$ μm. The gray and the black curves show the grain size distributions of samples taken from megaripples in Wadi Rum in southern Jordan. The average wavelength of these megaripples was 2.17 m, considerably larger than the Nahal Kasuy megaripples.

The grain size analysis of the samples taken from six saltation traps is shown in Fig. 11 and in Table 3. The median of the samples ranges from 135 to 207 μm, which is close to fine particle dimensions. Samples T-2 and T-4 comprised 36.8% and 25.5% particles, respectively, with grain diameters larger than 250 μm, whereas this percentage was smallest for T-6 (4.84%). Generally, although most of the grains moving in saltation are fine, a small fraction comprises coarse particles. We used these results in the following section to elucidate the mechanism by which coarse particles can be dislodged from megaripple crests.

3.3. Morphodynamics of megaripples in Plot D during storms

3.3.1. Megaripple dynamics under storm events

Three strong storms were recorded during our study (Fig. 8). Although each windstorm effected change on the landscape, the most dramatic change occurred in Plot D after the 27th February 2009 storm (Fig. 12), when exceptionally strong winds caused the megaripples to be broken down into normal ripples. Addressing megaripple dynamics, Bagnold (1941) predicted that megaripples will disappear and regular ripples will be formed when the coarse grains in the crest begin to saltate. This is probably what happened in Plot D. According to the rough estimation of the threshold velocity via Eq. 8, which is shown in Fig. 6 and is only applicable in the absence of saltation of fine particles, wind speeds above 15 m/s can drive the coarse grains (average diameter $d = 780$ μm and about 5% 1-mm grains) into saltation. We prefer to use Eq. 8 instead of Bagnold's formula (Eq. 7) as it seems to be more accurate and it has been used more frequently in recent studies (Jerolmack et al., 2006). The first storm of 27th February broke the crests into smaller segments and the second storm of 23rd March continued that trend, further breaking the megaripples down into normal ripples. Another important factor that contributed to the progressive disappearance of the megaripples is the fact that the two storms came from the same direction (west), making their effects cumulative. In contrast, we observed that when the wind's direction changes between storm events, the result will be

Table 2
The average ϕ ($\phi = \log_2 D$, where D is the grain diameter in mm) moments of megaripples at Nahal Kasuy (megaripples in Plot D, incipient megaripples, and normal ripples sampled on 5th February 2008), median (D_{50}), and the sample type as calculated and classified by GRADISTAT (Blott and Pye, 2001). The last table row shows the moments for the crest samples taken from two large megaripples at Wadi Rum in southern Jordan, 25th July 2008.

Sampling location	$(\bar{x}_\phi)$	σ_ϕ	Sk_ϕ	Kg_ϕ	Median	Sample type
	Mean	Sorting	Skewness	Kurtosis	$-$ D_{50} (μm)	
Nahal Kasuy megaripples crest (λ ~ 70 cm)	1.51	1.30 Poorly sorted	0.46 Finely skewed	3.07 Mesokurtic	368.8	Trimodal, poorly sorted
Incipient megaripples (λ ~ 15 cm)	1.91	1.08 Poorly sorted	0.01 Symmetrical	0.66 Very platykurtic	284.6	Polymodal, poorly sorted
Normal ripples (λ ~ 8 cm)	2.65	0.55 Moderately well sorted	1.60 Very finely skewed	17.90 Very leptokurtic	157.9	Unimodal, well sorted
Wadi Rum megaripples, crest (λ ~ 217 cm) Dune plinth	0.37	1.25 Poorly sorted	0.29 Symmetrical	1.64 Platykurtic	866.5	Bimodal, poorly sorted

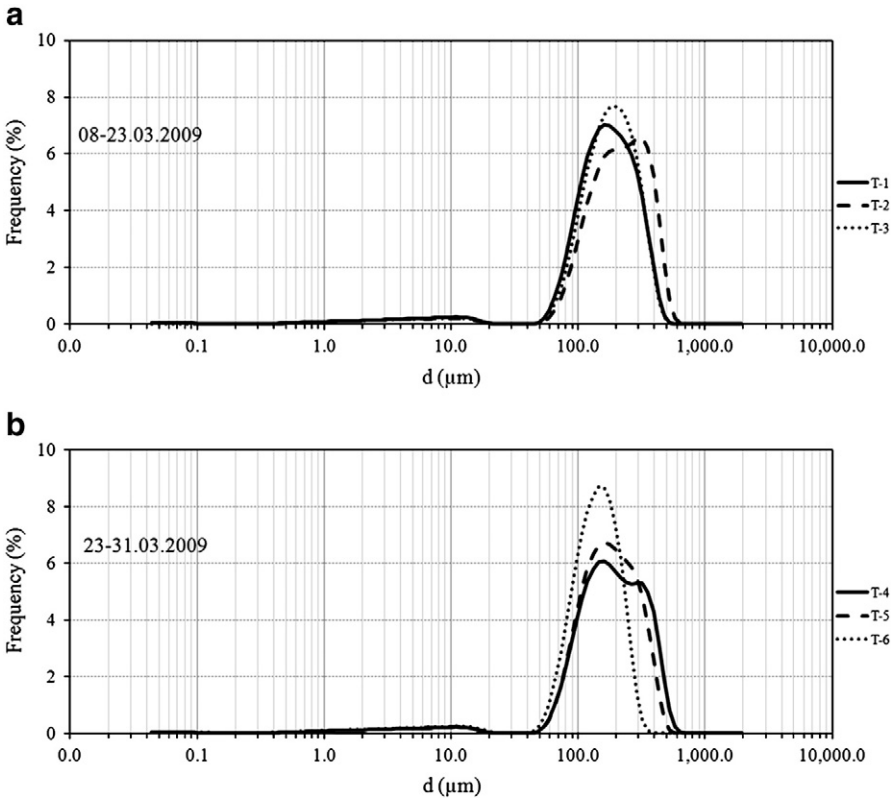

Fig. 11. Grain size distributions of sand from saltation traps during the unusually windy March of 2009. (a) Sand collected by traps, 8th–23rd March 2009. (b) Sand collected by traps, March 2009.

a complex pattern of megaripples (each with a broken crest-line) with smaller ripples extending in different directions between them. Wind statistics for the period that coincides with our visits between 20/2 and 31/3/09 are shown in Table 4. It is important to note that this period was the windiest during our three-year study, and therefore, its results show the largest creep mass of coarse particles (see calculation in Section 3.3.2).

The assumption that megaripples were broken down due to coarse grain saltation is supported by grain-size analyses of samples taken from Plot D (from ripple crests) before and after the storms (Fig. 13). The typical bimodal distribution of grain-sizes in megaripple crests was replaced after the storm by a unimodal distribution, like that which characterizes normal ripples.

Fig. 14 shows the progressive megaripple disappearance in Plot D from a different perspective. The effects of the 27th February storm are clearly shown in Fig. 15, where the average distance that each crest drifted downwind is indicated. These distances are proportional to DP for the period between the two successive visits.

Identical behavior was observed after the storm of 8th May 2008 (Fig. 16), but in that case the megaripples remained in the plot. The megaripples drifted smaller average distances downwind, their sinuosity was increased, and one megaripple was broken in half. Since only weak winds (DP = 0.7) were detected during the period immediately after 8th May, the megaripples remained virtually unchanged. Thus, one short storm event is not sufficient to destroy the megaripples, but instead, the cumulative force of several storms is needed. During the first stage of megaripple breakdown, the megaripples will become more sinuous wavier, after which the crests will undergo segmentation due to the presence of different drift velocities along the crest. In the final stage, strong winds continue to drive the coarse grains that protect the crests into saltation, and the megaripples slowly disappear, eventually being replaced by normal ripples. Over time, the newly formed normal ripples will probably develop again into megaripples as the smaller, normal ripples coalesce. The first stage of this process in Plot D is shown in Fig. 17.

Table 3
Grain size results of the saltation traps during March 2009.

Trap	Period	Location	Mean diameter [μm]	Mode [μm]	Median [μm]
T-1	8–23.3.09	Plot B	180.07	211.35	166.53
T-2	8–23.3.09	Plot B	222.74	218.33	207.29
T-3	8–23.3.09	Plot C	185.78	218.33	176.03
T-4	23–31.3.09	Plot C	203.78	162.98	178.69
T-5	23–31.3.09	Plot C	185.42	168.37	168.96
T-6	23–31.3.09	Plot C	139.40	157.77	135.80

Almost the same sequence of events observed in Plot D as a result of the two storms of 27th February and 23rd March 2009 also occurred in Plot B. The first storm broke the megaripples down into smaller segments, and the second storm almost destroyed all the megaripples in the plot, although the final effect was less dramatic than that observed in Plot D. The heightened sensitivity of the megaripples in Plot D to storms may have been because they were the highest in the field study, and thus, the coarse grains at their crests were exposed to higher wind shear stress, which may be able to directly lift the coarse particles (see discussion in Section 3.3.3). Indeed, on smaller megaripples, the wind shear stress was insufficient to bring the coarse grains into saltation, indicating that the smaller ripples may even grow during a storm event. According to Jackson and Hunt's model of flow over low hills (Jackson and Hunt, 1975), the bed shear stress is larger near the crest and becomes larger as the bedforms become higher (Pelletier, 2009). The interaction between flow, megaripple topography, and grain size at the crest controls ripple height.

We can obtain a rough estimation of the increase in the wind shear stress by using an approximation for the roughness length z_e over a surface covered with megaripples and under saltation (Pelletier, 2009). The velocity profile above the surface comprises two different

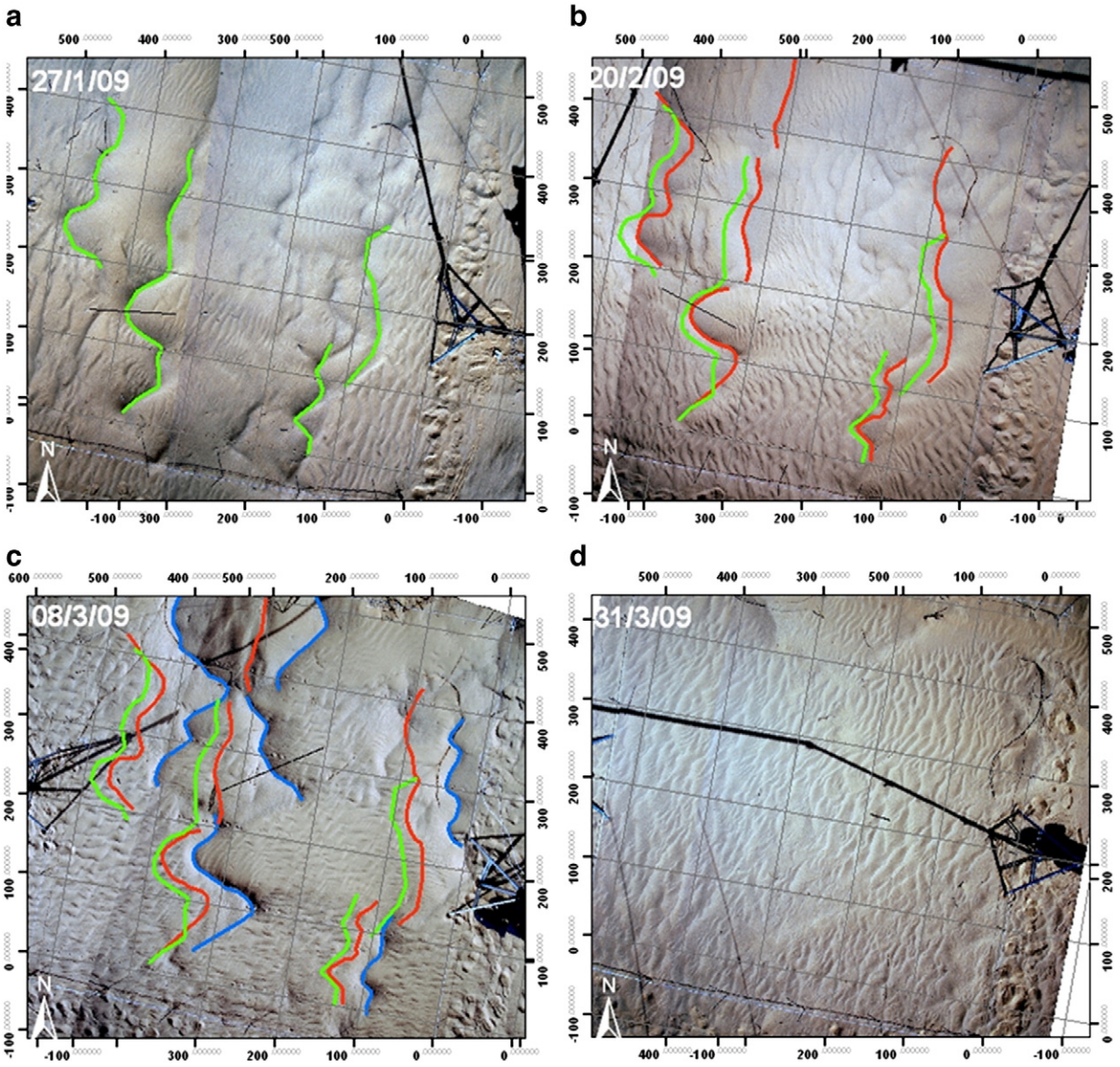

Fig. 12. Megaripple morphodynamics in plot D, February and March 2009. Due to the unusually large storms that occurred on 27th February and 23rd March, the megaripples were broken down into normal ripples. The colors correspond to the megaripple crests on successive visits (green — 27th January; red — 20th February; blue — 8th March). The prevailing wind direction was left to right and the grid was1 × 1 m.

dominant scales of roughness—one characterizes flow very close to the bed in the saltation layer and the other characterizes flow at a larger spatial scale over a rippled surface.

On a flat surface with active saltation, z_0 is a function of both the grain diameter and the excess shear velocity and is given by (Sherman, 1992):

$$z_0 = \frac{D}{15} + C_m \frac{(u_* - u_{*t})^2}{g} \tag{12}$$

Table 4
Wind data from Nahal Kasuy for the period 20/2–31/3/09. DP is the potential drift potential; RDP is resultant drift potential; RDD is RDP direction; RDP/DP is the wind directionality and *t* is the time (in percent) that the wind is above the fluid threshold for sand transport (taken as 6 m/s).

Period	DP	RDP	RDD	RDP/DP	t[%]
21/2–8/3-2009	12.99	10.85	251	0.83	18.2
9/3–23/3-2009	5.16	4.0	257	0.78	6.3
24/3–31/3-2009	1.83	1.74	252	0.95	1.0

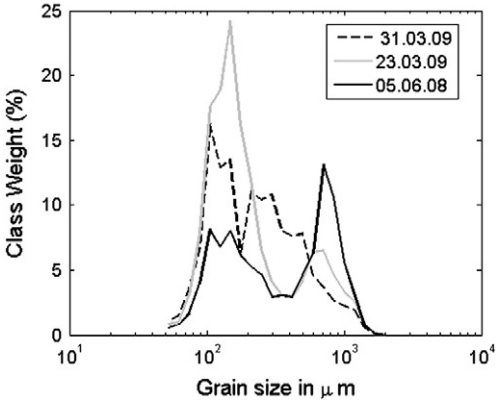

Fig. 13. Grain size analyses of crest samples taken before the storms (05.06.08), after the first storm (23rd March 2009) and after the second storm (31st March 2009). The typical bimodal distribution of megaripples changed to a unimodal distribution of normal ripples.

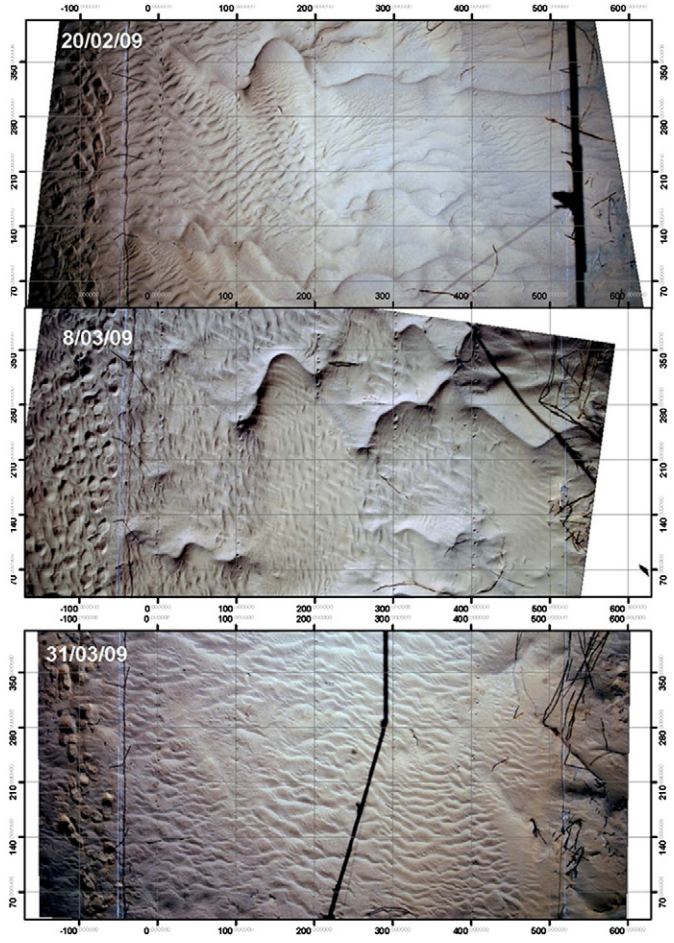

Fig. 14. Snapshots of plot D during the period between 20th February and 31st August 2009. The colors correspond to the crest-lines on successive visits (red — 27th January; blue — 20th February; green — 8th March). The large megaripples in this plot were destroyed by the strong storms, and new, small ripples took their place.

where $C_m = 0.136$ is an empirical constant, u_* is the shear velocity (assuming $u_* > u_{*t}$), and u_{*t}, given by Eq. 8, is 0.264 m/s for particles with $D = 0.2$ mm. Using $u_* = 0.5$ (which is close to the value of u_{*t} during the storms) gives $z_0 = 0.76$ mm. The effective roughness length over a rippled surface z_e can be approximated by (Pelletier, 2009):

$$z_e = z_0 \exp\left[\frac{1}{2}\left(\delta \ln\left(\frac{L}{z_0}\right)\right)^2\right] \tag{13}$$

where L is the half-length of the ripples at the half-length position (which is $\lambda/2$) and δ is the maximum slope of the ripples, which can be approximated by h/L where h is ripple height. Using $h = 7$ cm and $\lambda = 70$ cm gives $\delta = 0.2$, which is a realistic slope for the megaripples at Nahal Kasuy ($z_e = 1.6$ mm). Based on Jackson and Hunt's model (1975), variation in bed shear stress scales according to $\log_{10}(L/z_e)$ (see Fig. 3 in Pelletier, 2009). Using $\log_{10}(L/z_e) = 2.34$ shows that the bed shear stress near the crest will increase by approximately 80%. It is important to note that this estimation is very sensitive to the maximum bed slope δ (Pelletier, 2009). Taking, for example, $\delta = 0.3$ gives $\log_{10}(L/z_e) = 1.93$, which shows that the bed shear stress near the crest will increase by approximately 40%.

3.3.2. Creep mass flux

We used Eq. 5 to calculate the creep mass flux of the one large megaripple in Plot D (the second megaripple from the left in Fig. 16). Table 5 shows ripple migration rates during different periods. We used $p = 0.35$, $\rho = 2710$ kg/m^3, and $H = 5$ cm for the calculation. The computed creep mass flux is induced by the saltation flux that is proportional to the sand drift potential (Fryberger, 1979). Since the crest moved in the direction of RDP, we assume that q_c will be proportional to RDP as indicated by the results in Table 5. This computed creep flux is the time averaged during the period of measurement. If we want to compute the creep flux during the period the wind was above the saltation threshold, we need to take into account that t is the fraction of time the wind was above the fluid threshold and also that RDP/DP is the wind directionality, because only the flux in the direction of the resultant drift potential contributed to megaripple movement. For example, for the period between 20th February and 8th March 2009, $t = 0.182$ and RDP/DP = 0.83. Using these corrections gives $q_c = 6.23 \times 10^{-5}$ kg m^{-1} s^{-1}. $q_c = 6.23 \times 10^{-5}$ kg m^{-1} s^{-1} Zimbelman et al. (2009) obtained $q_c = 8 \times 10^{-5}$ kg m^{-1} s^{-1} $q_c = 8 \times 10^{-5}$ kg m^{-1} s^{-1} for

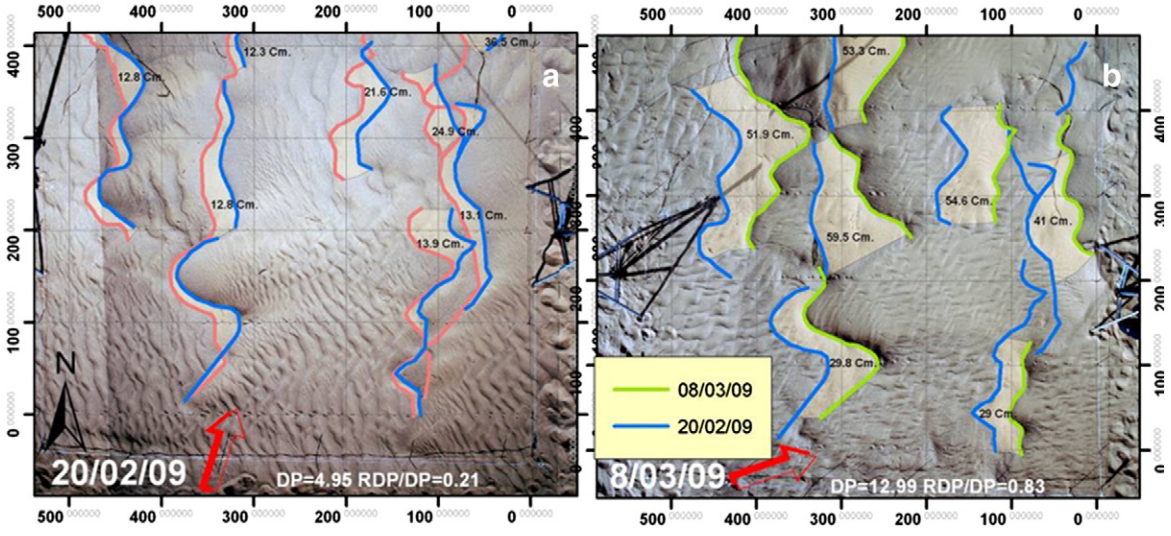

Fig. 15. Megaripple morphodynamics in Plot D during 20th February (a) 8 March 2009 (b) The colors correspond to the megaripple crests on two successive visits. The figure shows the effect of the storm of 27th February 2009 (the grid is 1 × 1 m).

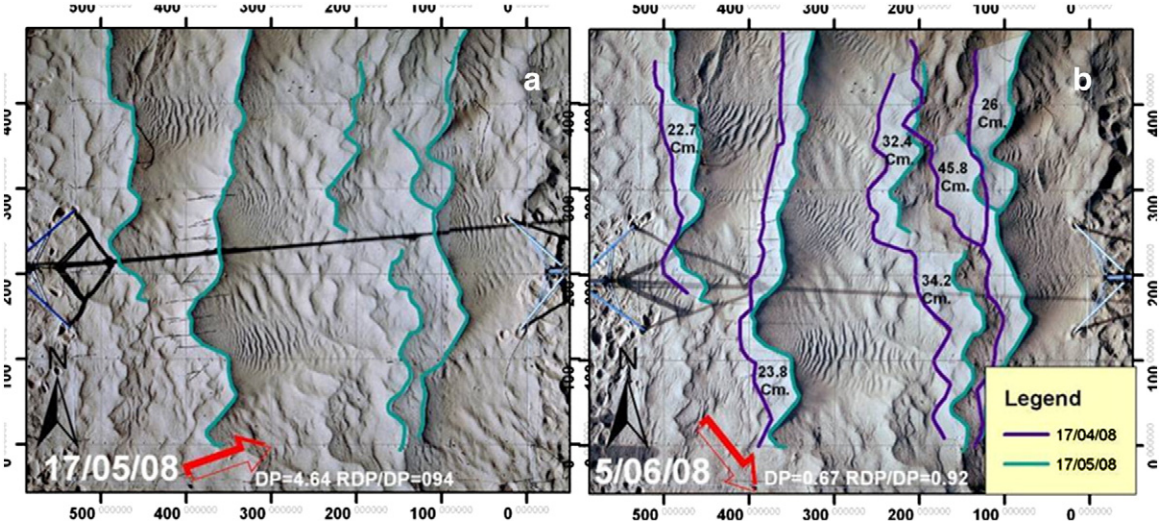

Fig. 16. Plot D before and after the storm of 8th May 2008. Panel (a) shows the location of megaripple crest-lines on 17th May. Panel (b) shows the crest lines both of 17th April and of 17th May. Note that there was almost no change during the period from 17th May to 5th June 2008 as DP was very low. The numbers between the two crest lines (panel b) indicate the average distance the megaripples moved downwind (the grid is 1×1 m).

3 cm-high granule ripples during a particularly strong wind event at the Great Sand Dunes National Park that was 28% higher than the creep mass flux in Nahal Kasuy, mainly because the wind was much stronger during the event that was measured by Zimbelman et al. (2009). This calculation assumes that ripple height remains constant during ripple migration. Taking into account that photogrammetry measurements of ripple height and migration are prone to error, subsequent creep flux calculations based on those ripple measurements may accrue as much as 30% error. The calculated creep mass flux can help to estimate the rate of movement of megaripples with different heights during storms in Nahal Kasuy and can also facilitate the development of reliable megaripple models (Yizhaq, 2005).

We can also estimate the number of coarse grains that moved across a unit of crest length per minute (Zimbelman et al., 2009), assuming that the granules on the advancing leeward slope are the primary contributor to the volume of the displaced ripple. For the period 20th February to 8th March 2009, the volume of sand that traveled per one centimeter length was $5 \times 29.8 \times 1$, or 149 cm^3, which is equivalent to 0.043 cm^3/min. If we assume that all the coarse grains are identical spheres, each with a diameter of 0.78 mm, and that grain porosity is 0.35, then we get 53 granules/min crossing each centimeter of ripple crest compared to 27 granules/min calculated for 1.5 mm diameter grains at the Great Sand Dunes National Park (Zimbelman et al., 2009). Note that the above calculation of creep flux is only a rough estimate, as it neglected the distribution of grain-size inherent in mixed soils, where a particle's chance of being ejected from the surface depends on its cross-sectional area (Rice et al., 1995).

3.3.3. Cause of megaripple flattening

The observed megaripple flattening that occurs during storm events must be preceded by the removal of the armoring layer of coarse particles on the crest. In fact, Bagnold (1941) already hypothesized that during strong wind events the armoring particles will be brought into saltation, causing the megaripples to be flattened, as we observed here for the first time. The question then becomes, what is the physical mechanism that brings the coarse particles into saltation at high wind speeds, ultimately causing the megaripples to flatten?

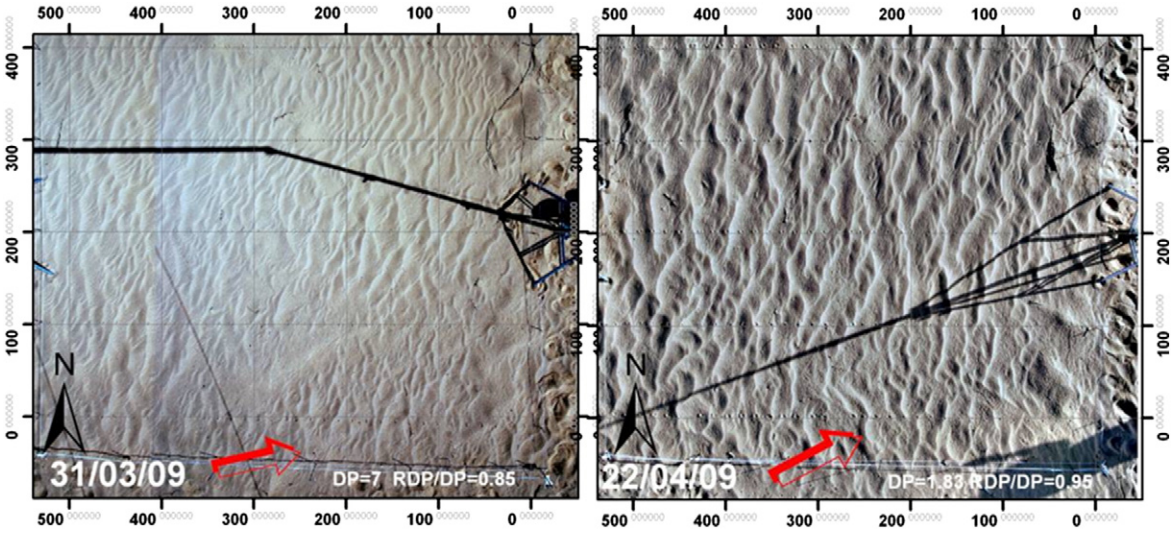

Fig. 17. Initial development of normal ripples in Plot D after megaripple destruction on 31st March 2009. The red arrows show the direction of RDP during the period between the previous and the current visits.

Table 5
Averaged creep mass flux at Nahal Kasuy.

Time	Number of days	t [%]	Average distance [m]	RDP [v.u.]	Averaged q_c [kg m^{-1} s^{-1}]
17/4/08–17/5/08	31	7.12	0.24	4.35	$1.78 \cdot 10^{-7}$
17/5/08–6/1/09	235	3.53	0.08	0.57	$3.91 \cdot 10^{-6}$
20/2/09–8/3/09	16	18.20	0.30	10.85	$9.49 \cdot 10^{-6}$

There are two mechanisms that can mobilize the coarse particles on the megaripple crests and bring them into saltation: direct lifting by fluid drag and indirect lifting due to the impacts of saltating particles ('splash'). For flat sand beds, theory and numerical models show that the absorption of wind shear stress by saltating particles reduces the wind stress at the surface to a value below the fluid threshold (e.g., Ungar and Haff, 1987; Werner, 1990; Anderson and Haff, 1991; Andreotti, 2004; Kok and Renno, 2009a, 2009b). Particles on the surface are thus sheltered from the wind, and the wind stress at the surface actually decreases as u_* increases above the fluid threshold. For a flat sand bed, coarse particles will thus not be lifted by fluid drag even for $u_* > u_{*t}$. However, this situation may differ at the megaripple crest, which protrudes into the saltation layer, thereby reducing the sheltering effect at the soil surface due to wind stress absorption by the saltating particles above. Field measurements made by Greeley et al. (1996) and Namikas (2003) and compiled in Fig. 5 from Kok and Renno (2009a) indicate that the mean saltation height for ~250-μm sand grains is ~3–4 cm. Since the height of the megaripples at Nahal Kasuy was about 5 cm, their crests likely protruded from the saltation layer, and as such, they would have experienced substantially higher wind shear stress than that felt in the troughs. As a consequence, an increase in u_* would thus produce an increase in the surface wind stress at the megaripple crest to the point that coarse particles could be lifted. For a given megaripple height, there thus exists a threshold shear velocity below which megaripples grow but above which the megaripples are flattened due to fluid entrainment of the coarse grains. Moreover, this mechanism implies a feedback between the height of the megaripple and the wind speed at which it is flattened: the higher the megaripple, the more it protrudes into the saltation layer, the higher the shear stress at the crest surface at a given u_*, and thus, the lower the critical u_* at which coarse particles can be lifted by the fluid. This effect seems to explain why the high megaripples disappeared during the storms while the smaller megaripples often did not. Moreover, this effect implies that megaripple height, which was believed to grow indefinitely (Bagnold, 1941) is self-limiting, and it also explains the positive correlation between maximum grain size at the crest and the wavelength. This point is further addressed in the next subsection.

3.3.3.1. Numerical simulations of bi-dispersed particles. In addition to the direct fluid lifting mechanism hypothesized in the previous section, particles on the ripple crest could also be mobilized by splashing, which dominates particle lifting during steady-state saltation over flat sand beds (Ungar and Haff, 1987; Werner, 1990; Anderson and Haff, 1991; Kok and Renno, 2009a, 2009b). To test this hypothesis, we used the recently developed numerical saltation model COMSALT (Kok and Renno, 2009a, 2009b). COMSALT includes many of the advances of previous numerical saltation models (e.g., Werner, 1990), and in addition, it includes (1) a physically based parameterization of the splashing of surface particles that is in good agreement with experimental and numerical studies, (2) a generalization of this splashing process to beds of mixed particle sizes, and (3) a detailed treatment of the influence of turbulence on particle trajectories, which agrees with laboratory measurements. Partially because of these advances, COMSALT can reproduce a much wider range of measurements than any previous numerical saltation model (Kok and Renno, 2009a, 2009b). COMSALT has also recently been used to show that saltation can be maintained on Mars by wind speeds an order of magnitude less than that required to initiate it (Kok, 2010a, 2010b).

We used COMSALT to simulate sand transport over a flat sand bed comprising equal surface fractions of fine (180 μm) and coarse (700 μm) particles. The simulation results confirmed our experimental findings (Fig. 11) that the 180 μm particles are the predominant saltators (Fig. 18). Because the coarse particles are about four times larger and thus almost two orders of magnitude heavier than the fine particles, impacts from the 180 μm saltators will mainly cause the coarse particles to move in microscopic hops in the creep transport mode. The fact that the fractional contribution of the coarse particles to the mass flux is less than 0.1 is an indication that the coarse grains rarely saltate. Only unusually high impact speeds can cause the 700 μm particles to enter saltation.

As wind speed increases, the mean speed of impacting saltating particles stays approximately constant (Ungar and Haff, 1987; Andreotti, 2004; Creyssels et al., 2009; Kok and Renno, 2009a, 2009b; Kok, 2010a, 2010b), but the probability distribution of impact speeds widens (Fig. 19). The cause of this is the increasing difference in typical fluid speeds between the bottom of the saltation layer (where fluid speeds decrease with u_*) and the top of the saltation layer (where fluid speeds increase strongly with u_*). This effect is evident both in measurements (see, for example, Fig. 4 in Bagnold, 1938) and in numerical models (see, for example, Fig. 3 in Ungar and Haff, 1987, and Fig. 12 in Kok and Renno, 2009a, 2009b). The increasing wind speeds near the top of the saltation layer cause the population of fast-moving particles to grow, such that the chance of an unusually high saltator impact speed (say, >5 m/s) increases drastically with u_* (Fig. 19). This, in turn, causes an increasing fraction of the saltator impacts to splash coarse particles into saltation. Hence, the fraction of the streamwise mass flux that is due to the coarse fraction increases strongly with wind speed (Fig. 18) by about $\sim u_*^{3.7}$. Nevertheless, for $u_* \approx 0.5$ m/s, which is representative of the winds during the storms in Nahal Kasuy, only ~0.1% of the mass flux is due to the coarse fraction. This may explain why more than one storm was needed to remove the coarse grains from the ripple crests and flatten the megaripples.

We have thus identified two possible mechanisms that could cause megaripple flattening at high wind speeds: (1) direct fluid entrainment of the coarse particles on the crests of high megaripples that protrude into the saltation layer and therefore experience a greater fluid drag at the soil surface, and (2) the splashing of coarse particles into saltation by the high-speed tail of the probability distribution of

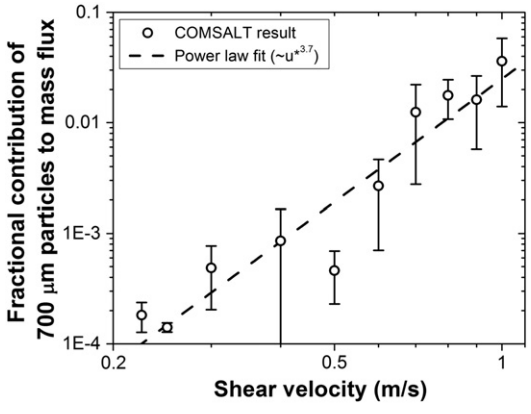

Fig. 18. The fractional contribution of 700 μm particles to the streamwise mass flux over a soil bed with equal surface fractions of 180 and 700 μm particles, simulated with the numerical saltation model COMSALT (Kok and Renno, 2009a). Each data point denotes the average and standard error of eight separate simulations that generated varying results because of the stochastic nature of COMSALT (Kok and Renno, 2009a). The dashed line denotes a least squares power law fit to the simulation results.

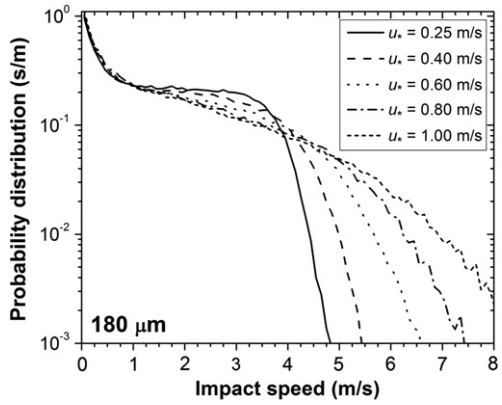

Fig. 19. Probability distribution of the impact speed of 180 μm particles saltating over a soil bed with equal surface fractions of 180 and 700 μm particles, simulated with the numerical saltation model COMSALT (Kok and Renno, 2009a). Shown are simulations at $u_* = 0.25$, 0.40, 0.60, 0.80, and 1.00 m/s (solid, dashed, dotted, dash-dotted, and short dashed lines, respectively).

the saltator impact speed, which increases sharply with increasing wind speed. The direct fluid entrainment mechanism also explains why the larger (and thus higher) megaripples were flattened while the smaller megaripples often were not affected. Further field measurements and targeted wind tunnel experiments could help determine which of these two mechanisms dominates.

4. Conclusions

We present here the findings of 3 years of research in the megaripple field at Nahal Kasuy in the southern Negev. During the study period, the wind drift potential exhibited a low absolute value that was also small relative to its values in former years. Grain-size analysis from different parts of the megaripples and from normal ripples show that a bimodal mixture of grain sizes is needed for megaripple formation and that the coarse particles are more abundant at the crest. The coarse grains that protect the crest enable the ripple to grow, but as the ripple height becomes too large the bed shear stress increases and the wind can move the armoring layer more easily. In addition, during storms there is a higher probability that high velocity fine particles will splash coarse grains into saltation. When this happens (during strong storms), the megaripple will flatten and even disappear as we observed in the field. Megaripple flattening requires either sustained winds above the fluid threshold for a sufficient length of time or a series of storms, all of which blow from the same direction. The Weibull distribution density function for a specific site can be used to predict the probability of megaripples being flattened by strong storms. It is clear that for large megaripples, the probability for flattening by the wind is very small. As a result, these larger megaripples will last for very long periods of time.

Megaripples will continue to develop until they have reached a balance between the available grain-sizes and the wind at the specific site. In Nahal Kasuy, the megaripple building process will continue as long as the wind is above the fluid threshold of the fine particles and below the fluid threshold of the coarse grains (6 m/s$<U<$15 m/s at a height of 3.3 m for Nahal Kasuy). Under these conditions, only fine grains saltate. According to our results, the two most important parameters in the control of megaripples spatio-temporal dynamics are DP and the grain-size distribution. We calculated the bed creep mass induced by the saltation of fine particles ($q_c = 6.23\times10^{-5}$ kg m^{-1} s^{-1}), and it is in the range of values that were calculated at other locations (Jerolmack et al., 2006; Zimbelman et al., 2009). Does megaripple growth continue without saturation (Manukyan and Prigozhin, 2009), or does it eventually become saturated due to the removal of the coarse particles by the wind? More field observations from other locations with larger megaripples using better mathematical models are needed to answer this question.

The megaripples in Nahal Kasuy are small compared to those found at other sites, such as in Jordan or Brazil. The advantage of the Nahal Kasuy megaripples for field study is that the time scale of their development is approximately one to two years. They are sensitive to wind action and their patterns can change quickly after the strong storms typical of the area in the winter and spring. This sensitivity to wind action casts doubts on Bagnold's (1941) suggestion that megaripple dimensions vary according to the square root of their age. Taking into account the variability in wind direction and the annual variability in wind power (DP) and the complex interaction between megaripples and wind, it is hard to believe that Bagnold's simple relation exists.

However, it is clear that elucidation of the long-term development of huge megaripples ($\lambda = 44$ m), such as those in the Carachi Pampa, Argentina (Milana, 2009), can be effectively achieved only via mathematical modeling, which will include insights gained from field studies such as that reported here. For massive megaripples (e.g., Carachi Pampa, Argentina), it is not even clear whether the same mechanism of impact ripples is responsible for their formation, or, as suggested by Milana (2009) their evolution is related to the aerodynamic instabilities of the saltation curtain–air interface.

Acknowledgements

This work was supported by the Israel Science Foundation (grant N531/06). We thank Prof. Yosef Ashkenazy for providing the wind data from Uvda airport, Mr. Roy Talbi for helping us with the wind measurements at Nahal Kasuy, Ms. Roni Bluestein for the map preparations and for the reviewers Matt Balme and Bernard O. Bauer for their excellent comments which improved the clarity of the manuscript.

References

Anderson, R.S., Haff, P.K., 1988. Simulation of eolian saltation. Science 241, 820–823.
Anderson, R.S., Haff, P.K., 1991. Wind modification and bed response during saltation of sand in air. Acta Mechanica Supplement 1, 21–51.
Andreotti, B., 2004. A two-species model of aeolian sand transport. Journal of Fluid Mechanics 510, 47–70.
Bagnold, R.A., 1938. The measurement of sand storms. Proceedings of the Royal Society of London Series. A—Mathematical and Physical Sciences 167 (A929), 0282–0291.
Bagnold, R.A., 1941. The Physics of Blown Sand and Desert Dunes. Methuen, London.
Balme, M., Berman, D.C., Bourke, M.C., Zimbelman, J.R., 2008. Transverse Aeolian Ridges (TARs) on Mars. Geomorphology 101, 703–720.
Blott, S.J., Pye, K., 2001. GRADISTAT: a grain size distribution and statistics package for the analysis for unconsolidated sediments. Earth Surface Processes and Landforms 26, 1237–1248.
Bullard, J.E., 1997. A note on the use of the "Fryberger method" for evaluating potential sand transport by wind. Sedimentary Research 67, 499–501.
Creyssels, M., Dupont, P., Ould el Moctar, A., Valance, A., Cantat, I., Jenkins, J.T., Pasini, J.M., Rasmussen, K.R., 2009. Saltating particles in a turbulent boundary layer: experiment and theory. Journal of Fluid Mechanics 625, 47–74.
Defoe, O.K., Compton, A.H., 1925. The density of rock salt and calcite. Physical Review 25, 618–620.
El-Baz, F., 1986. The formation and motion of dunes and sand seas. In: El-Baz, F., Hassan, M.H.A. (Eds.), Physics of Desertification. Martinus Nijhoff Publishers, Dordrecht, the Netherlands, pp. 78–79.
Ellwood, J.M., Evans, P.D., Wilson, I.G., 1975. Small scale aeolian bedforms. Journal of Sedimentary Petrology 45, 554–561.
Fenton, J.D., Abbott, J.E., 1977. Initial movement of grains on a stream bed: the effect of relative protrusion. Proceedings of the Royal Society of London 352A, 523–537.
Fryberger, S.G., 1979. Dune forms and wind regime. In: McKee, E.D. (Ed.), A Study of Global Sand Seas: U.S. Geological Survey Profile Pap. 1052, Washington, pp. 137–169.
Fryberger, S.G., Hesp, P., Hastings, K., 1992. Aeolian granule deposits, Namibia. Sedimentology 39, 319–331.
Ginat, H., 1991. The Geology and Geomorphology of the Yotvata Region. Thesis submitted for the degree of Master of Science. The Hebrew University of Jerusalem (In Hebrew).
Goldreich, Y., 1998. The Climate of Israel: Observations, Research and Applications. Bar-Ilan Press, Ramat Gan.
Greeley, R., Iversen, J.D., 1985. Wind as a Geological Process on Earth, Mars, Venus and Titan. Cambridge University Press, London.
Greeley, R., Blumberg, D.G., Williams, S.H., 1996. Field measurements of the flux and speed of wind-blown sand. Sedimentology 43, 41–52.

Jackson, P.S., Hunt, J.C.R., 1975. Turbulent wind flow over a low hill. Quarterly Journal of the Royal Meteorological Society 101, 929–955.
Jerolmack, D.J., Mohrig, D., Grotzinger, J.P., Fike, D., Watters, W.A., 2006. Spatial grain size sorting in aeolian ripples and estimation of wind conditions on planetary surfaces: application to Meridiani Planum, Mars. Journal of Geophysical Research 111, E12S02. doi:10.1029/2005JE002544.
Jimenez, J.A., Maia, L.P., Serra, J., Morais, J., 1999. Aeolian dune migration along the Cearà coast, north-eastern Brazil. Sedimentology 46, 689–701.
Kok, J.F., 2010a. Differences in the wind speeds required for initiation versus continuation of sand transport on Mars: implications for dunes and sand storms. Physical Review Letters 104, 074502.
Kok, J.F., 2010b. An improved parameterization of wind-blown sand flux on Mars that includes the effect of hysteresis. Geophysical Research Letters 37, L12202.
Kok, J.F., Renno, N.O., 2009a. A comprehensive numerical model of steady-state saltation (COMSALT). Journal of Geophysical Research-Atmospheres 114, D17204.
Kok, J.F., Renno, N.O., 2009b. Electrostatics in wind-blown sand. Physical Review Letters 100, 014501.
Levin, N., Ben-Dor, E., 2004. Monitoring sand dune stabilization along the coastal dunes of Ashdod-Nizanim, Israel, 1945–1999. Journal of Arid Environments 58, 335–355.
Manukyan, E., Prigozhin, L., 2009. Formation of aeolian ripples and sand sorting. Physical Review E 79, 031303.
Manwell, J.F., McGowan, A.L., Rogers, A.L., 2009. Wind Energy Explained. Wiley, Chippenham, Wiltshire, U.K.
Milana, J.P., 2009. Largest wind ripples on Earth. Geology 37, 343–346.
Mountney, N.G., Russell, A.J., 2004. Sedimentology of cold-climate aeolian sandsheet deposits in the Askja region of northeast Iceland. Sedimentology 166, 223–244.
Namikas, S.L., 2003. Field measurement and numerical modelling of aeolian mass flux distributions on a sandy beach. Sedimentology 50, 303–326.
Pelletier, J.D., 2009. Controls of the height and spacing of aeolian ripples and transverse dunes: a numerical modeling investigation. Geomorphology 105, 322–329.
Pye, K., Tsoar, H., 2009. Aeolian Sands and Sand Dunes. Springer-Verlag, Berlin Heidelberg.
Raudkivi, A.J., Ettema, R., 1982. Stability of armour layers in rivers. Journal of the Hydraulics Division 108, 1047–1057.
Rice, M.A., Willets, B.B., Mckewan, I.K., 1995. An experimental study of multiple grain-size ejecta produced by collisions of saltating grains with a flat bed. Sedimentology 42, 695–706.
Rubin, D.M., 2006. Ripple effect: unforeseen applications of sand studies. Eos 87 (30), 293 297.
Sakamoto-Arnold, C.M., 1988. Eolian features produced by the December 1977 windstorm, Southern San Joaquin Valley, California. Journal of Geology 89, 129–137.
Shao, Y., Lu, H., 2000. A simple expression for wind erosion threshold friction velocity. Journal of Geophysical Research 105, 22,437–22,443.
Sharp, R.P., 1963. Wind ripples. Journal of Geology 71, 617–636.
Sherman, D.J., 1992. An equilibrium relationship for shear velocity and apparent roughness length in aeolian saltation. Geomorphology 5, 419–431.
Stone, R.O., Summers, H.J., 1972. Study of subaqueous and subareial sand ripples. US Office of Naval Research, Final Report. USC Geology 72-1, Arlington, Virginia. 274 pp.
Tsoar, H., 1990. Grain-size characteristics of wind ripples on a desert seif dune. Geography Research Forum 10, 37–50.
Ungar, J.E., Haff, P.K., 1987. Steady-state saltation in air. Sedimentology 34, 289–299.
Walker, D.J. 1981. An Experimental Study of Wind Ripples. Unpublished Masters Thesis. Massachusetts Institute of Technology, Cambridge, Mass.
Werner, B.T., 1990. A steady-state model of wind-blown sand transport. Journal of Geology 98, 1–17.
Wiberg, P.L., Smith, J.D., 1987. Calculations of the critical shear stress for motion of uniform and heterogenous sediments. Water Resources Research 23, 1471–1480.
Williams, S.H., Zimbelman, J.R., Ward, A.W., 2002. Large ripples on earth and Mars. 33rd Lunar and Planetary Science Conference. 1508.pdf.
Yizhaq, H., 2005. A mathematical model for aeolian megaripples on Mars. Physica A 357, 57–63.
Yizhaq, H., 2008. Aeolian megaripples: mathematical model and numerical simulations. Journal of Coastal Research 24, 1369–1378.
Yizhaq, H., Isenberg, O., Wenkart, R., Tsoar, H., Karnieli, A., 2009. Morphology and dynamics of aeolian megaripples in Nahal Kasuy, Southern Israel. Israel Journal of Earth Sciences 57, 145–161.
Zimbelman, J.R., Irwin III, R.P., Williams, S.H., Bunch, F., Valdez, A., Stevens, S., 2009. The rate of granule ripple movement on Earth and Mars. Icarus 203, 71–76.